# Adaptive nonseparable vector lifting scheme for digital holographic data compression

Yafei Xing, Mounir Kaaniche, Béatrice Pesquet-Popescu, Frédéric Dufaux

# Adaptive non separable vector lifting scheme for digital holographic data compression

Yafei Xing,[1,*] Mounir Kaaniche,[2] Béatrice Pesquet-Popescu,[1] and Frédéric Dufaux[1]

[1]*Institut Mines-Télécom, Télécom ParisTech, CNRS LTCI, 37-39 Rue Dareau, Paris, France, 75014*

[2]*Université Paris 13, Sorbonne Paris Cité, L2TI-Institut Galilée, 99 avenue J. B. Clément, Villetaneuse, France, 93430*

compiled: December 5, 2014

Holographic data plays a crucial role in the recent three dimensional imaging as well as microscopic applications. As a result, huge amounts of storage capacity will be involved for this kind of data. Therefore, it becomes necessary to develop efficient hologram compression schemes for storage and transmission purposes. In this paper, we focus on the shifted distance information, obtained by the phase shifting algorithm, where two sets of difference data need to be encoded. More precisely, a non separable vector lifting scheme is investigated in order to exploit the two-dimensional characteristics of the holographic contents. Simulations performed on different digital holograms have shown the effectiveness of the proposed method in terms of bitrate saving and quality of object reconstruction.

*OCIS codes:* (090.1760) Holography, Computer holography; (100.2000) Digital image processing.

http://dx.doi.org/10.1364/XX.99.099999

## 1. Introduction

Digital holography (DH) [1, 2] has attracted a considerable attention in recent years due to its interest in various application fields such as 3D imaging [3], microscopy [4, 5] and object contouring [6, 7]. However, in optical DH, digital holograms are recorded under very strict physical environments. As a result, a technique, called computer generated holography (CGH) [8, 9], can alternatively simulate the whole recording and reconstruction procedure.

With the aim of mathematically generating object wavefront at the hologram plane, the key point for synthesizing CGH consists in designing the model of the object as well as the geometry of wave propagation. It decides the computational burden and influences the reconstruction quality. Generally, the geometry of wave propagation is related to the selected object model. Ray tracing method is commonly used for 3D objects consisting of scatter points [10], obtained by tracing the ray from point sources to the hologram plane. Also, thanks to high-speed calculation techniques, it makes possible the application on objects with high-density point distribution [11]. On the other hand, with the advantages of fast Fourier transform, another method based on wave optics is becoming the major calculation trend of CGH. It can be adapted to most of the object models, e.g., polygonal mesh models [12, 13], or projection images based models [14]. Whatever the retained method, the interference patterns are then obtained by superposing the interference of object wave and reference wave.

Nevertheless, in numerical reconstruction, conventional in-line setup [15] or off-axis setup [16] with single reference wave recording makes the reconstructed images suffer from zero-order image and twin image. To overcome this problem, in-line phase-shifting digital holography (PSDH) has been proposed by Yamaguchi [17], and records three holograms using the reference wave with stepwise changed phase to reconstruct the complex amplitude of the object wave. Assuming that, a full-parallax CGH is composed

* Corresponding author: xing@enst.fr

of many elemental holograms obtained from different viewpoints of objects, the storage burden is increased by a factor 3 under the phase-shifting scheme. Therefore, compressing digital holographic data effectively is a crucial issue, especially with phase-shifting.

To this end, we should first note that the encoding process can be applied based on different representations of holographic data such as the interference patterns, the complex amplitude with real and imaginary part information, the amplitude and phase information and shifted distance information. Lossy compression technique based on subsampling, quantization and discrete Fourier transform is developed in [18]. Mills and Yamaguchi introduced quantization to interference patterns in [19]. The results provide useful insight for holographic data reduction but also reveal that application of only quantization is not efficient, because the resulting quality falls rapidly as the number of bits decreases. To overcome this drawback, it has been proposed in [20] to apply wavelet transform to digital holograms followed by thresholding and quantization. Nonuniform quantization of digital holograms has also been investigated in [21]. The effectiveness of standard JPEG and JPEG2000 compression techniques on interference patterns has also been demonstrated for optically recorded DH [22] and CGH [23] where JPEG2000 was found to be more performant. In [24], Darakis proposed a method based on Fresnelets transform. The complex amplitude is firstly decomposed to Fresnelets coefficients and then the real and imaginary part of each subband are quantized. The efficiency of adaptive scalar quantization has been also studied for the amplitude and phase information obtained from DH [25] and CGH [26], and it has been concluded that phase information contributes more to the reconstruction quality than amplitude information. In a recent work [27], we have shown that it is more interesting to encode two sets of difference data called shifted distance information. Moreover, according to our previous studies [26, 27], we have observed that the obtained shifted distance information are more correlated, and so, they can be efficiently encoded by using joint coding schemes. To this respect, a separable vector lifting-based decomposition has been recently developed in [28]. A significant gain has been achieved compared to the state-of-the-art independent coding scheme.

However, according to the visual patterns of shifted distance information, the separable vector lifting scheme (VLS) developed recently in [28] is not so efficient to cope with the two dimensional isotropic characteristics of the input data. For this reason, we propose in this paper to investigate a *non separable* VLS-based decomposition well *adapted* to the hologram contents. While a similar non separable decomposition has been recently presented in a preliminary work for stereo image coding purpose [29], the current one aims at adapting such structure for holographic data compression applications. More precisely, since this data presents repetitive circular structures similar to waves, we propose to study the impact of using longer lengths of the prediction lifting operator. To this respect, and in order to develop a general framework, we provide the explicit expressions of the spatial supports of the different operators whatever the retained lengths. Moreover, the prediction filter coefficients will be optimized by minimizing the variance of the detail signal in order to reduce the complexity of the proposed decomposition.
The remainder of this paper is organized as follows. In Section 2, the main issues regarding PSDH and conventional separable VLS are addressed. Then, the proposed hologram coding method is described in Section 3. Finally, experimental results are given and discussed in Section 4 and conclusions are drawn in Section 5.

## 2. Related works

### 2.A. Computer generated phase-shifting holography

The Fresnel holograms are generated based on the setup illustrated in Fig. 1(a). The wave propagation is simplified in the coordinate system as shown in Fig. 1(b). Let us denote by $(x', y')$ the location of the object points in the object plane. Using Fresnel transform, the complex amplitude of object wave $U(x, y)$ at the hologram plane can be approximated by Eq. (1):

$$U(x,y) = \exp[\, i\frac{\pi}{\lambda d}(x^2+y^2)] \times \mathscr{F}\{U_o(x',y')\exp[\, i\frac{\pi}{\lambda d}(x')^2+(y')^2]\}, \quad (1)$$

where $\mathscr{F}$ represents the Fourier transform, $U_o(x', y')$ denotes the complex amplitude of the object point, $\lambda$ denotes the wavelength of the laser beam and $d$ is the distance between the object plane and the hologram plane $(d > 0)$. Thus,

three Fresnel holograms are then obtained by computing the intensity of the interference patterns as follows:

$$I_H(x,y;\phi) = |U_R(x,y;\phi)+U(x,y)|^2,\ \phi \in \{0, \frac{\pi}{2}, \pi\}, \quad (2)$$

where $U_R$ is the complex amplitude of the reference wave and $\phi$ is the stepped phase.
In order to reconstruct the pure complex object wave at the hologram plane, a three-step phase shifting algorithm [30] can be employed:

$$\widehat{U}(x,y) = \frac{1-i}{4U_R^*}\{I_H(x,y;0) - I_H(x,y;\frac{\pi}{2}) + i[I_H(x,y;\frac{\pi}{2}) - I_H(x,y;\pi)]\}, \quad (3)$$

where $U_R^*$ is the conjugate of the reference wave with $\phi = 0$.
After that, image reconstruction is achieved by applying the inverse Fresnel transformation of the derived complex amplitude $\widehat{U}(x,y)$.

### 2.B. Shifted distance information-based coding scheme

According to Eq. (3), the object wave reconstruction requires the knowledge of the three interference pattern intensities $I_H(x,y;0)$, $I_H(x,y;\frac{\pi}{2})$ and $I_H(x,y;\pi)$. In the context of hologram compression, instead of encoding these three patterns, it is more efficient to encode two sets of difference data, referred to as shifted distance information [27], given by:

$$\begin{cases} D^{(1)}(x,y) = I_H(x,y;0) - I_H(x,y;\frac{\pi}{2}) \\ D^{(2)}(x,y) = I_H(x,y;\frac{\pi}{2}) - I_H(x,y;\pi). \end{cases} \quad (4)$$

In a previous work, standard image coding tools such as JPEG and JPEG2000 have been used to encode *separately* $D^{(1)}$ and $D^{(2)}$. However, an important feature of the holographic data is the presence of correlation between the interference patterns since they are obtained from the wavefronts emanating from the same 3D object. Indeed, as it can be seen in Fig. 2 which displays the two resulting images $(D^{(1)}, D^{(2)})$ associated to the "Bunny-1" object shown in Fig. 3, it is clear that these images present similar visual contents. Note that the correlation existing between $D^{(1)}$ and $D^{(2)}$ has been demonstrated in [28] by using the entropy measure.

For this reason, we have proposed recently to encode *jointly* $D^{(1)}$ and $D^{(2)}$ by applying the VLS in order to exploit the dependencies existing between them [28]. In what follows, we give the main issues on the previous separable VLS-based hologram compression method.

### 2.C. VLS-based joint coding scheme

First, we should note here that VLS has been found to be an efficient joint encoding scheme for correlated inputs such as the multispectral images and stereo data [31, 32]. A generic VLS is illustrated by Fig. 4.

More precisely, one image (for example $D^{(1)}$) is selected as a reference image and encoded independently of the other image. To this end, a classical lifting structure [33], composed of a prediction and an update step, is applied to $D^{(1)}$ to generate its detail and approximation wavelet coefficients. Then, the second image $D^{(2)}$ is encoded by exploiting the correlation between the two images. Thus, a prediction and update steps are firstly performed to compute the approximation coefficients of $D^{(2)}$. After that, a hybrid prediction stage, which uses the information coming from the reference image $D^{(1)}$, is added to produce the detail coefficients of $D^{(2)}$.
This decomposition is applied along the lines of $D^{(1)}$ and $D^{(2)}$ leading to a detail and an approximation subbands for each image. Then, the same process is performed on the columns of both resulting subbands yielding the horizontal, vertical and diagonal detail subbands as well as the approximation one.

## 3. Proposed adaptive hologram compression technique

### 3.A. Motivation

As mentioned before, it is important to note that the previous decomposition is handled in a separable manner by simply applying a one dimensional (1D)-VLS along the lines, then along the columns of the holographic data. However, according to the visual contents of the generated patterns, it can be observed from Fig. 2 that the input images $(D^{(1)}, D^{(2)})$ present rather isotropic structures. Therefore, the previous developed separable VLS is not optimal, and it becomes more important to design a non separable decomposition, designated in what follows by NS-VLS, in order to *simultaneously* exploit the correlation existing between the shifted distance information data as well as their two-dimensional (2D) wave characteristics.

### 3.B. NS-VLS decomposition

Since our decomposition is based on the concept of a multiresolution transform, we will describe the NS-VLS for a given resolution level $j$. Note that $j = 0$ corresponds to the initial images $D^{(1)}$ and $D^{(2)}$ (i.e the full resolution). In the following, $D_j^{(1)}$ and $D_j^{(2)}$ designate the approximation coefficients of $D^{(1)}$ and $D^{(2)}$ at each resolution level $j$ and have the dimensions of the initial images divided by $2^j$ along the horizontal and vertical dimensions. Moreover, at each pixel location $(x, y)$, the approximation coefficients of the first (resp. second) image $D_j^{(1)}(x, y)$ (resp. $D_j^{(2)}(x, y)$) are divided into four polyphase components denoted by

$$\begin{cases} D_{0,j}^{(i)}(x,y) = D_j^{(i)}(2x, 2y), \\ D_{1,j}^{(i)}(x,y) = D_j^{(i)}(2x, 2y+1), \\ D_{2,j}^{(i)}(x,y) = D_j^{(i)}(2x+1, 2y), \\ D_{3,j}^{(i)}(x,y) = D_j^{(i)}(2x+1, 2y+1), \end{cases} \tag{5}$$

where $i \in \{1, 2\}$.

Fig. 5 illustrates the NS-VLS analysis structure. As shown in Fig. 5, one image (here $D^{(1)}$) is selected as a reference image and encoded independently of the other one. To this end, a classical non separable lifting structure [34], composed of three prediction steps and an update one, is applied to $D_j^{(1)}$ in order to generate the detail signals oriented diagonally $D_{j+1}^{(HH,1)}$, vertically $D_{j+1}^{(LH,1)}$ and horizontally $D_{j+1}^{(HL,1)}$, as well as the approximation one $D_{j+1}^{(1)}$. Thus, the output wavelet coefficients, at the resolution level $(j + 1)$, can be written as follows:

$$D_{j+1}^{(HH,1)}(x,y) = D_{3,j}^{(1)}(x,y) - \Big((\mathbf{P}_{0,j}^{(HH,1)})^\top \mathbf{D}_{0,j}^{(HH,1)} + (\mathbf{P}_{1,j}^{(HH,1)})^\top \mathbf{D}_{1,j}^{(HH,1)} + (\mathbf{P}_{2,j}^{(HH,1)})^\top \mathbf{D}_{2,j}^{(HH,1)}\Big), \tag{6}$$

$$D_{j+1}^{(LH,1)}(x,y) = D_{2,j}^{(1)}(x,y) - \Big((\mathbf{P}_{0,j}^{(LH,1)})^\top \mathbf{D}_{0,j}^{(LH,1)} + (\mathbf{P}_{1,j}^{(LH,1)})^\top \underline{\mathbf{D}}_{j+1}^{(HH,1)}\Big), \tag{7}$$

$$D_{j+1}^{(HL,1)}(x,y) = D_{1,j}^{(1)}(x,y) - \Big((\mathbf{P}_{0,j}^{(HL,1)})^\top \mathbf{D}_{0,j}^{(HL,1)} + (\mathbf{P}_{1,j}^{(HL,1)})^\top \overline{\mathbf{D}}_{j+1}^{(HH,1)}\Big), \tag{8}$$

$$D_{j+1}^{(1)}(x,y) = D_{0,j}^{(1)}(x,y) + \Big((\mathbf{U}_{0,j}^{(HL,1)})^\top \mathbf{D}_{j+1}^{(HL,1)} + (\mathbf{U}_{1,j}^{(LH,1)})^\top \mathbf{D}_{j+1}^{(LH,1)} + (\mathbf{U}_{2,j}^{(HH,1)})^\top \mathbf{D}_{j+1}^{(HH,1)}\Big), \tag{9}$$

where for every $i \in \{0, 1, 2\}$ and $o \in \{HL, LH, HH\}$,

- $\mathbf{P}_{i,j}^{(o,1)} = (p_{i,j}^{(o,1)}(s,t))_{(s,t)\in\mathcal{P}_{i,j}^{(o,1)}}$ represents the prediction weighting vector whose support is denoted by $\mathcal{P}_{i,j}^{(o,1)}$.
- $\mathbf{D}_{i,j}^{(o,1)} = (D_{i,j}^{(1)}(x+s, y+t))_{(s,t)\in\mathcal{P}_{i,j}^{(o,1)}}$ is a reference vector used to compute $D_{j+1}^{(o,1)}(x, y)$.
- $\underline{\mathbf{D}}_{j+1}^{(HH,1)} = (D_{j+1}^{(HH,1)}(x+s, y+t))_{(s,t)\in\mathcal{P}_{1,j}^{(LH,1)}}$ and $\overline{\mathbf{D}}_{j+1}^{(HH,1)} = (D_{j+1}^{(HH,1)}(x+s, y+t))_{(s,t)\in\mathcal{P}_{1,j}^{(HL,1)}}$ correspond to two reference vectors used in the second and the third prediction steps, respectively.
- $\mathbf{U}_{i,j}^{(o,1)} = (u_{i,j}^{(o,1)}(s,t))_{(s,t)\in\mathcal{U}_{i,j}^{(o,1)}}$ is the update vector coefficients whose support is designated by $\mathcal{U}_{i,j}^{(o,1)}$.
- $\mathbf{D}_{j+1}^{(o,1)} = (D_{j+1}^{(o,1)}(x+s, y+t))_{(s,t)\in\mathcal{U}_{i,j}^{(o,1)}}$ is the reference vector containing the set of detail samples used in the update step.

For the second image $D_j^{(2)}$, selected as a target one, a joint wavelet decomposition is performed by taking into account its correlation with the reference one $D_j^{(1)}$. More specifically, a lifting structure, similar to that used with $D_j^{(1)}$, is firstly applied on $D_j^{(2)}$ in order to produce three intermediate detail signals $\widetilde{D}_{j+1}^{(HH,2)}$, $\widetilde{D}_{j+1}^{(LH,2)}$ and $\widetilde{D}_{j+1}^{(HL,2)}$, which will be used to compute the approximation coefficients $D_{j+1}^{(2)}$. Then, a second prediction stage is added. Indeed, three hybrid prediction steps, which aim at exploiting simultaneously the intra and inter-image redundancies, are applied in order to generate the final detail coefficients $D_{j+1}^{(HH,2)}$, $D_{j+1}^{(LH,2)}$ and $D_{j+1}^{(HL,2)}$. Therefore, compared to a classical lifting structure, the main feature of a VLS concerns the prediction step which uses samples from the same image $D_j^{(2)}$ and also their corresponding ones taken from the reference one $D_j^{(1)}$. Thus, the final detail wavelet coefficients, at the resolution

level $(j+1)$, are expressed as follows:

$$D_{j+1}^{(HH,2)}(x,y) = \widetilde{D}_{j+1}^{(HH,2)}(x,y) - \Big((\mathbf{Q}_{0,j}^{(HH,2)})^\top \widetilde{\mathbf{D}}_{0,j+1}^{(HH,2)} + (\mathbf{Q}_{1,j}^{(HH,2)})^\top \widetilde{\mathbf{D}}_{1,j+1}^{(HH,2)} + (\mathbf{Q}_{2,j}^{(HH,2)})^\top \widetilde{\mathbf{D}}_{2,j+1}^{(HH,2)} + (\mathbf{P}_{0,j}^{(HH,1,2)})^\top \mathbf{D}_{0,j}^{(HH,1)} + (\mathbf{P}_{1,j}^{(HH,1,2)})^\top \mathbf{D}_{1,j}^{(HH,1)} + (\mathbf{P}_{2,j}^{(HH,1,2)})^\top \mathbf{D}_{2,j}^{(HH,1)} + (\mathbf{P}_{3,j}^{(HH,1,2)})^\top \mathbf{D}_{3,j}^{(HH,1)}\Big), \quad (10)$$

$$D_{j+1}^{(LH,2)}(x,y) = \widetilde{D}_{j+1}^{(LH,2)}(x,y) - \Big((\mathbf{Q}_{0,j}^{(LH,2)})^\top \widetilde{\mathbf{D}}_{0,j+1}^{(LH,2)} + (\mathbf{Q}_{1,j}^{(LH,2)})^\top \underline{\mathbf{D}}_{j+1}^{(HH,2)} + (\mathbf{P}_{0,j}^{(LH,1,2)})^\top \mathbf{D}_{0,j}^{(LH,1)} + (\mathbf{P}_{2,j}^{(LH,1,2)})^\top \mathbf{D}_{2,j}^{(LH,1)}\Big), \quad (11)$$

$$D_{j+1}^{(HL,2)}(x,y) = \widetilde{D}_{j+1}^{(HL,2)}(x,y) - \Big((\mathbf{Q}_{0,j}^{(HL,2)})^\top \widetilde{\mathbf{D}}_{0,j+1}^{(HL,2)} + (\mathbf{Q}_{1,j}^{(HL,2)})^\top \overline{\mathbf{D}}_{j+1}^{(HH,2)} + (\mathbf{P}_{0,j}^{(HL,1,2)})^\top \mathbf{D}_{0,j}^{(HL,1)} + (\mathbf{P}_{1,j}^{(HL,1,2)})^\top \mathbf{D}_{1,j}^{(HL,1)}\Big), \quad (12)$$

where for every $i \in \{0,1,2,3\}$ and $o \in \{HL, LH, HH\}$,

- $\mathbf{Q}_{i,j}^{(o,2)} = (q_{i,j}^{(o,2)}(s,t))_{(s,t)\in\mathcal{Q}_{i,j}^{(o,2)}}$ is the intra prediction weighting vector whose support is designated by $\mathcal{Q}_{i,j}^{(o,2)}$.
- $\mathbf{P}_{i,j}^{(o,1,2)} = (p_{i,j}^{(o,1,2)}(s,t))_{(s,t)\in\mathcal{P}_{i,j}^{(o,1,2)}}$ is the hybrid prediction weighting vector whose support is denoted by $\mathcal{P}_{i,j}^{(o,1,2)}$.
- $\widetilde{\mathbf{D}}_{0,j+1}^{(o,2)} = (D_{j+1}^{(2)}(x+s,y+t))_{(s,t)\in\mathcal{Q}_{0,j}^{(o,2)}}$ is a reference vector containing the approximation coefficients $D_{j+1}^{(2)}$ used to compute the detail ones $D_{j+1}^{(o,2)}(x,y)$.
- $\widetilde{\mathbf{D}}_{1,j+1}^{(HH,2)} = (\widetilde{D}_{j+1}^{(HL,2)}(x+s,y+t))_{(s,t)\in\mathcal{Q}_{1,j}^{(HH,2)}}$ and $\widetilde{\mathbf{D}}_{2,j+1}^{(HH,2)} = (\widetilde{D}_{j+1}^{(LH,2)}(x+s,y+t))_{(s,t)\in\mathcal{Q}_{2,j}^{(HH,2)}}$ are two reference vectors, containing respectively the intermediate detail coefficients $\widetilde{D}_{j+1}^{(HL,2)}$ and $\widetilde{D}_{j+1}^{(LH,2)}$, used to compute the final detail coefficients $D_{j+1}^{(HH,2)}(x,y)$.
- $\underline{\mathbf{D}}_{j+1}^{(HH,2)} = (D_{j+1}^{(HH,2)}(x+s,y+t))_{(s,t)\in\mathcal{Q}_{1,j}^{(LH,2)}}$ and $\overline{\mathbf{D}}_{j+1}^{(HH,2)} = (D_{j+1}^{(HH,2)}(x+s,y+t))_{(s,t)\in\mathcal{Q}_{1,j}^{(HL,2)}}$ are two intra prediction vectors used to compute $D_{j+1}^{(LH,2)}(x,y)$ and $D_{j+1}^{(HL,2)}(x,y)$.
- $\mathbf{D}_{i,j}^{(o,1)} = (D_{i,j}^{(1)}(x+s,y+t))_{(s,t)\in\mathcal{P}_{i,j}^{(o,1,2)}}$ is a vector containing some samples of the reference image $D_j^{(1)}$ used to exploit the inter-image redundancies during the computation of the final detail coefficients $D_{j+1}^{(o,2)}(x,y)$.

By repeating the same decomposition strategy on the approximation subbands over $J$ resolution levels, two multiresolution representations of $D^{(1)}$ and $D^{(2)}$ are obtained. Finally, at the last resolution level $J$, instead of encoding the approximation subband of the target image $D_J^{(2)}$, it would be interesting to exploit its correlation with $D_J^{(1)}$ and thus to encode the following residual subband $e_J^{(2)}$:

$$e_J^{(2)}(x,y) = D_J^{(2)}(x,y) - p_J^{(1,2)} D_J^{(1)}(x,y). \quad (13)$$

where $p_J^{(1,2)}$ is an hybrid prediction coefficient that exploits the correlation between $D_J^{(2)}$ and $D_J^{(1)}$.

### 3.C. Design of prediction and update filters

To effectively exploit the correlation existing between the repetitive circular structures of the holograms, it would be interesting to consider longer lengths of the lifting operators. To this end, we address in what follows the retained optimization techniques as well as the sets of the spatial supports for any given size of the prediction and update filters. The transmission cost of the involved filter coefficients will also be discussed.

#### 3.C.1. Optimization techniques

With the ultimate aim of designing an NS-VLS-based decomposition well adapted to the contents of the holographic data, the different prediction filters $\mathbf{P}_j^{(o,1)}$ (with $o \in \{HH, LH, HL\}$), used to generate the detail subbands $D_{j+1}^{(o,1)}$, will be optimized at each resolution level by minimizing the variance of the detail coefficients. After that, the update filter is optimized by minimizing the square error between the approximation coefficients $D_{j+1}^{(1)}$ and the decimated version of the signal resulting from an ideal low-pass filter.

Then, for the second image $D^{(2)}$, all the prediction and update operators can also be optimized by adopting the same strategy used with

$D^{(1)}$. However, since $D^{(1)}$ and $D^{(2)}$ present similar contents, the optimization process of the first three prediction filters $\mathbf{P}_j^{(o,2)}$ and the update one $\mathbf{U}_j^{(2)}$ can be omitted by imposing these operators to be equal to those obtained with $D^{(1)}$. Thus, we have:

$$\begin{aligned}&\mathbf{P}_j^{(HH,2)} = \mathbf{P}_j^{(HH,1)}, \mathbf{P}_j^{(LH,2)} = \mathbf{P}_j^{(LH,1)},\\ &\mathbf{P}_j^{(HL,2)} = \mathbf{P}_j^{(HL,1)}, \mathbf{U}_j^{(2)} = \mathbf{U}_j^{(1)}.\end{aligned} \tag{14}$$

Note that this procedure presents the advantages of simplifying the optimization strategy and reducing the overhead cost corresponding to the number of filter coefficients that must be sent to the decoder. Finally, for the remaining hybrid prediction filters $\mathbf{P}_j^{(o,1,2)}$ and $\mathbf{Q}_j^{(o,2)}$, they will be optimized by minimizing the variance of the detail coefficients $D_{j+1}^{(o,2)}$.

Based on $\ell_2$ minimization criteria, we should note here that the optimization techniques used to design the prediction and update filters were found to be efficient and fast since their optimal solutions can be simply obtained by solving a linear system of equations. For instance, by taking an hologram of size $600 \times 600$ and using an Intel core 2 (3 GHz) computer with a Matlab implementation, the optimization of the update filter with length parameter $L_u = 2$ requires $0.23s$ whereas that of the prediction filters with length parameter $Lp = 2$ (resp. $L_p = 12$) takes about $0.13s$ (resp. $1.65s$).

### 3.C.2. Definition of the spatial supports

To apply the considered adaptive NS-VLS, we should define the sets of spatial supports for the different prediction and update filters. To this end, it is important to note here that it has been shown in [34] that a classical separable lifting structure with 1D prediction and update filters, of length $L_p$ and $L_u$ respectively (which often take even values), has an equivalent 2D structure similar to that shown in the top side of Fig. 5 (i.e the block which is applied on $D^{(1)}$). More specifically, this results in choosing the following spatial supports of the prediction and update operators used with $D^{(1)}$:

$$\begin{aligned}\mathcal{P}_{0,j}^{(HH,1)} = \{(s,t) \in \mathbf{Z}^2 \mid &-\frac{L_p}{2}+1 \le s \le \frac{L_p}{2}\\ \text{and} \quad &-\frac{L_p}{2}+1 \le t \le \frac{L_p}{2}\},\end{aligned} \tag{15}$$

$$\mathcal{P}_{1,j}^{(HH,1)} = \mathcal{P}_{0,j}^{(LH,1)} = \{(s,0) \mid -\frac{L_p}{2}+1 \le s \le \frac{L_p}{2}\}, \tag{16}$$

$$\mathcal{P}_{2,j}^{(HH,1)} = \mathcal{P}_{0,j}^{(HL,1)} = \{(0,t) \mid -\frac{L_p}{2}+1 \le t \le \frac{L_p}{2}\}, \tag{17}$$

$$\mathcal{U}_{0,j}^{(HL,1)} = \mathcal{P}_{1,j}^{(LH,1)} = \{(0,t) \mid -\frac{L_u}{2} \le t \le \frac{L_u}{2}-1\}, \tag{18}$$

$$\mathcal{U}_{1,j}^{(LH,1)} = \mathcal{P}_{1,j}^{(HL,1)} = \{(s,0) \mid -\frac{L_u}{2} \le s \le \frac{L_u}{2}-1\}, \tag{19}$$

$$\begin{aligned}\mathcal{U}_{2,j}^{(HH,1)} = \{(s,t) \in \mathbf{Z}^2 \mid &-\frac{L_u}{2} \le s \le \frac{L_u}{2}-1\\ \text{and} \quad &-\frac{L_u}{2} \le t \le \frac{L_u}{2}-1\}.\end{aligned} \tag{20}$$

While the same spatial supports are used with the three intra-prediction filters $\mathcal{P}_{i,j}^{(o,2)}$ and the update one $\mathcal{U}_{i,j}^{(o,2)}$ thanks to (14), those of the remaining hybrid prediction operators are given by:

$$\mathcal{Q}_{0,j}^{(HH,2)} = \{(0,0);(0,1);(1,0);(1,1)\}, \tag{21}$$

$$\mathcal{Q}_{1,j}^{(HH,2)} = \mathcal{Q}_{0,j}^{(LH,2)} = \{(0,0);(1,0)\}, \tag{22}$$

$$\mathcal{Q}_{2,j}^{(HH,2)} = \mathcal{Q}_{0,j}^{(HL,2)} = \{(0,0);(0,1)\}, \tag{23}$$

$$\begin{aligned}&\mathcal{P}_{0,j}^{(HH,1,2)} = \mathcal{P}_{0,j}^{(HH,1)}, \ \mathcal{P}_{1,j}^{(HH,1,2)} = \mathcal{P}_{1,j}^{(HH,1)},\\ &\mathcal{P}_{2,j}^{(HH,1,2)} = \mathcal{P}_{2,j}^{(HH,1)},\end{aligned} \tag{24}$$

$$\mathcal{P}_{1,j}^{(HL,1,2)} = \mathcal{P}_{2,j}^{(LH,1,2)} = \mathcal{P}_{3,j}^{(HH,1,2)} = \{(0,0)\}, \tag{25}$$

$$\mathcal{Q}_{1,j}^{(LH,2)} = \{(0,0);(0,-1)\}, \tag{26}$$

$$\mathcal{Q}_{1,j}^{(HL,2)} = \{(0,0);(-1,0)\}, \tag{27}$$

$$\mathcal{P}_{0,j}^{(LH,1,2)} = \mathcal{P}_{0,j}^{(LH,1)}, \ \mathcal{P}_{0,j}^{(HL,1,2)} = \mathcal{P}_{0,j}^{(HL,1)}. \tag{28}$$

Once the spatial supports are defined and the prediction and update coefficients are optimized, the latter must be transmitted to the decoder in order to proceed to the inverse transform and reconstruct the data $(D^{(1)}, D^{(2)})$. Knowing that the filter coefficients can be generally stored on 24 bits, the overhead cost related to the encoding of all the filter coefficients is given by:

$$o = \frac{L \times J \times 24}{2MN} \text{ bits per pixel (bpp)}, \qquad (29)$$

where $L$ is the number of filter coefficients in the proposed NS-VLS, $J$ is the number of resolution levels, and $M \times N$ is the size of the data.
According to the defined sets of the spatial prediction and update supports, it can be checked that the involved number of coefficients is:

$$L = 2L_p^2 + 8L_p + L_u^2 + 4L_u + 19. \qquad (30)$$

For example, when $M = N = 600$ and $J = 3$, taking short length filters with parameters $L_p = 6$ and $L_u = 2$ results in a very small transmission cost equal to $0.015$ bpp. However, this overhead becomes more important and reaches $0.233$ bpp when $L_p = 32$ and $L_u = 2$.

## 4. Experimental results

### 4.A. Setup of Computer Generated Holography

For the sake of simplicity, elemental Fresnel holograms, generated by six projection images of four virtual 3D objects (shown in Fig. 3), are selected as the compression target in this paper. We should note here that the data is computer generated, since we deal with Computer Generated Phase Shifting Holography (CGPSH). In a numerical synthesis of CGH, Eq. (1) is discretized to:

$$U(k,l) = \exp[\, i\frac{\pi}{\lambda d}(k^2(\Delta x')^2 + l^2(\Delta y')^2)] \\ * \mathscr{F}\{\widehat{U}_o(m,n)\exp[\, i\frac{\pi}{\lambda d}(m^2\Delta x^2 + n^2\Delta y^2)]\}, \qquad (31)$$

where $k = 1, 2, ..., N_x$, $l = 1, 2, ..., N_y$ and $m = 1, 2, ..., N_x$, $n = 1, 2, ..., N_y$ represent the discrete dimensions' indices of the hologram and object planes, respectively; $\Delta x$, $\Delta y$ and $\Delta x'$, $\Delta y'$ are the horizontal and vertical sampling intervals of the hologram and object planes, respectively. Table. 1 gives the parameters used in the experimental results.

Table 1. Parameters of CGPSH

| | |
|---|---|
| laser wavelength | $\lambda = 630nm$ |
| distance of two planes | $d = 0.55m$ |
| dimension of plane | $5.5mm \times 5.5mm$ |
| number of samples | $N_x \times N_y = 600 \times 600$ |

### 4.B. Results and discussions

In order to illustrate the efficiency of the proposed hologram coding scheme, we shall compare it with state-of-the-art methods.

The first one represents the state-of-the-art coding method where the data $(D^{(1)}, D^{(2)})$ are separately encoded by using the JPEG2000 standard with the 9/7 wavelet transform. This independent coding scheme will be designated by "Independent". It is important to note here that this scheme has been considered as a reference method because it has already shown in [27] that it is more performant than the conventional hologram compression scheme where the three interference patterns are separately encoded [22].

The second approach, denoted in what follows by "Standard" corresponds to the standard joint coding scheme used often to exploit the inter-image redundancies in the context of stereo and video compression. Recall that its main idea consists in selecting one image (here $D^{(1)}$) as a reference one and encoding it in intra-mode. Then, the image error between $D^{(2)}$ and $D^{(1)}$ is encoded rather than the original one $D^{(2)}$. To encode the image error as well as $D^{(1)}$, the JPEG2000 with the 9/7 transform is used.

The third method corresponds to our previous joint hologram compression scheme based on the separable VLS [28]. This decomposition, designated by SEP-VLS(2,2), is performed by using a prediction and an update filters of size 2 (i.e $L_p = L_u = 2$).

Finally, we consider the proposed non separable extension of this scheme. This latter will be denoted by NS-VLS(2,2). We should note that all these multiresolution coding schemes have been carried out over 3 resolution levels (i.e $J = 3$).

All these methods are firstly compared in terms of Rate-Distortion (R-D) performance. Fig. 6 illustrates the PSNR of the reconstructed objects versus the bitrate given in bits per pixel (bpp). The obtained R-D curves show that the proposed NS-VLS-based method outperforms all the conventional coding schemes. For instance,

compared to the SEP-VLS(2,2) decomposition, the proposed non separable one achieves an improvement of about 0.3 to 1 dB depending on the object.

Moreover, Fig. 7 displays the reconstructed "Luigi" object for different coding schemes and provides the quality of reconstruction in terms of PSNR and the perceptual criterion Structural SIMilarity (SSIM) [35]. It is clear that the proposed NS-VLS(2,2) leads to better visual quality of reconstruction than the SEP-VLS(2,2) and the independent hologram compression method.

Furthermore, the relative gain of NS-VLS(2,2) compared to SEP-VLS(2,2) has also been measured by Bjontegaard metric [36]. The results are given in Table 2 for bitrate range from 0.3 bpp to 1.0 bpp. Thus, it can be noticed that the two approaches lead to similar performances in terms of the SSIM criterion since their corresponding gain is around zero (the values range from -0.01 to 0.02). However, the two other criteria confirm better the interest of the proposed approach, and show that NS-VLS(2,2) outperforms SEP-VLS(2,2) up to 10% and 0.8 dB in terms of bitrate saving and PSNR of the reconstructed objects, respectively.

Table 2. The average PSNR, SSIM and bitrate saving gains of NS-VLS(2,2) with respect to SEP-VLS(2,2) using Bjontegaard metric.

| Objects | bitrate saving (in %) | PSNR gain (in dB) | bitrate saving (in %) | SSIM gain |
|---|---|---|---|---|
| Bunny-1 | -4.79 | 0.40 | 2.98 | -0.004 |
| Bunny-2 | -9.33 | 0.62 | 4.20 | -0.014 |
| Luigi-1 | -10.30 | 0.80 | -9.59 | 0.026 |
| Luigi-2 | -5.26 | 0.43 | -7.75 | 0.022 |
| Girl | -3.13 | 0.30 | -10.79 | 0.018 |
| Teapot | -9.92 | 0.69 | 0.05 | -0.0002 |

In addition, due to the advantages of the NS-VLS, we have also tested this decomposition with different prediction filter lengths $L_p$. Indeed, increasing $L_p$ may be interesting for two reasons. The first one is explained by the fact that the holographic data presents repetitive circular structures similar to the propagation of waves. The second one is due to the objective of VLS which consists in exploiting the inter-images redundancies through the prediction stage. Thus, we propose in what follows to vary the length of the prediction filter while keeping the size of the update one fix (i.e $L_u = 2$). To this respect, in addition to the previous case given by $L_p = 2$, we take also $L_p \in \{6, 12, 20, 32\}$. Similarly to the notation NS-VLS(2,2), the new structures will be designated by NS-VLS(6,2), NS-VLS(12,2), NS-VLS(20,2) and NS-VLS(32,2).

Fig. 8 illustrates the R-D performance for different 3D objects. Compared to the case $L_p = 2$, it can be observed that increasing this length up to 12 or 20 leads to the good compression performance. Indeed, an important gain of about 10 dB is achieved by NS-VLS(12,2) and NS-VLS(20,2) compared to NS-VLS(2,2). Moreover, it can be also noticed that using very long filters ($L_p = 32$) leads to worse performance at low bitrate because of the expensive cost of encoding the filter coefficients compared to the case of small $L_p$ values.

We illustrate an example of R-D curves, shown in Fig. 9, where the coding cost of filter coefficients is not taken into account. As expected, it can be seen in this case that NS-VLS(32,2) becomes more performant and have R-D results close to that obtained by NS-VLS(20,2).

Fig. 10 shows the visual reconstruction quality of the object "Teapot" at 0.8 bpp using various NS-VLS schemes. Therefore, a NS-VLS with a prediction filter length of around 12 is efficient for compressing shifted distance information.

Finally, the Bjontegaard metric results shown in Table 3 demonstrates also the interest of NS-VLS(12,2) compared to the NS-VLS(2,2). Indeed, it shows a significant gain that reaches 80%, 12 dB and 0.29 in terms of bitrate saving, PSNR and SSIM, respectively.

All these results confirm the effectiveness of the proposed adaptive non separable VLS scheme for hologram compression purpose.

## 5. Conclusion and future work

In this paper, we have focused on the compression issue of the holographic data. To this end, a non separable vector lifting scheme has been developed to encode the phase-shifting holographic information in order to better exploit the 2D isotropic characteristics of this data. Moreover, the proposed decomposition has been adapted to the data contents. Due to the particular structures of such data, we have shown that increasing the prediction filter length results in a significant gain in terms of bitrate saving and visual quality of reconstruction.

As a future work, it would be interesting to extend the proposed approach to the digital holographic video coding framework. Moreover, while the standard PSNR and SSIM criteria have been used in this work, the quality assessment of the reconstructed objects could also be investigated by designing other metrics more appropriate for holographic data.

Table 3. The average PSNR, SSIM and bitrate saving gains of NS-VLS(12,2) with respect to NS-VLS(2,2) using Bjontegaard metric.

| Objects | bitrate saving (in %) | PSNR gain (in dB) | bitrate saving (in %) | SSIM gain |
|---|---|---|---|---|
| Bunny-1 | -72.80 | 11.21 | -66.89 | 0.13 |
| Bunny-2 | -78.84 | 12.22 | -80.20 | 0.25 |
| Luigi-1 | -72.34 | 11.52 | -68.96 | 0.18 |
| Luigi-2 | -74.33 | 11.78 | -71.95 | 0.17 |
| Girl | -69.18 | 8.55 | -62.71 | 0.08 |
| Teapot | -77.99 | 12.17 | -89.34 | 0.29 |

## References


[1] U. Schnars and W. Jüptner, "Direct recording of holograms by a CCD target and numerical reconstruction," *Applied Optics* **33**(2), 179–181 (1994).

[2] J. W. Goodman and R. W. Lawrence, "Digital image formation from electronically detected holograms," *Applied Physics Letters* **11**(3), 77–79 (1967).

[3] B. Javidi, P. Ferraro, S.-H. Hong, S. D. Nicola, A. Finizio, D. Alfieri, and G. Pierattini, "Three-dimensional image fusion by use of multiwavelength digital holography," *Optics Letters* **30**(2), 144-146 (2005).

[4] M. R. McCartney and D. J. Smith, "Electron Holography: Phase Imaging with Nanometer Resolution," *Annual Review of Materials Science* **37**, 729–767 (2007).

[5] M. K. Kim, "Principles and techniques of digital holographic microscopy," *SPIE Reviews,* **1**(1), 018005 (2010).

[6] J. R. Varner, "Holographic contouring: Alternatives and applications," *Proc. SPIE, Developments in Holography II,* **25** (1971).

[7] C. Quan, H. Shang, C. Tay, and P. Bryanston-Cross, "Holographic contouring using double-source technique and fourier transform analysis," *Optics and Lasers in Engineering* **30**(3-4), 351 – 362 (1998).

[8] W. J. Dallas, "Computer-generated holograms," in *The Computer in Optical Research*, B. Frieden, Ed., *Topics in Applied Physics* **41**, 291–366, Springer Berlin Heidelberg (1980).

[9] G. Tricoles, "Computer generated holograms: an historical review," *Applied Optics* **26**(20), 4351–4360 (1987).

[10] A. D. Stein, Z. Wang, and J. S. Leigh, "Computer-generated holograms: A simplified ray-tracing approach," in *Computers in Physics*, **6**(4), 389–392 (1992).

[11] N. Masuda, T. Ito, T. Tanaka, A. Shiraki, and T. Sugie, "Computer generated holography using a graphics processing unit," *Optics Express* **14**(2), 603–608 (2006).

[12] H. Kim, J. Hahn, and B. Lee, "Mathematical modeling of triangle-mesh-modeled three-dimensional surface objects for digital holography," *Applied Optics* **47**(19), D117–D127 (2008).

[13] K. Matsushima and S. Nakahara, "Extremely high-definition full-parallax computer-generated hologram created by the polygon-based method," *Applied Optics* **48**(34), H54–H63 (2009).

[14] J.-H. Park, M.-S. Kim, G. Baasantseren, and N. Kim, "Fresnel and fourier hologram generation using orthographic projection images," *Optics Express* **17**(8), 6320–6334 (2009).

[15] D. Gabor, "A new microscopic principle," *Nature* **161**(4098), 777–778 (1948).

[16] E. N. Leith and J. Upatnieks, "Reconstructed wavefronts and communication theory," *Journal of the Optical Society of America* **52**(10), 1123–1128 (1962).

[17] I. Yamaguchi and T. Zhang, "Phase-shifting digital holography," *Optics Letters* **22**(16), 1268–1270 (1997).

[18] T. J. Naughton, Y. Frauel, B. Javidi and E. Tajahuerce, "Compression of digital holograms for three-dimensional object reconstruction and recognition," *Applied Optics* **41**(20), 4124–4132 (2002).

[19] G. A. Mills and I. Yamaguchi, "Effects of quantization in phase-shifting digital holography," *Applied Optics* **44**(16), 1216–1225 (2005).

[20] A. E. Shortt, T. J. Naughton and B. Javidi, "Compression of digital holograms of three-dimensional objects using wavelets," *Optics Express* **14**(7), 2625–2630 (2006).

[21] A. E. Shortt, T. J. Naughton and B. Javidi, 'A companding approach for nonuniform quantization of digital holograms of three-dimensional objects," *Optics Express* **14**(12), 5129–5134 (2006).

[22] E. Darakis and J. J. Soraghan, "Compression of interference patterns with application to

phase-shifting digital holography," *Applied Optics* **45**(11), 2437–2443 (2006).

[23] Y. Xing, B. Pesquet-Popescu, and F. Dufaux, "Compression of computer generated hologram based on phase-shifting algorithm," in *European Workshop on visual information Processing*, 172-177, (Paris, France) (2013).

[24] E. Darakis and J. Soraghan, "Use of fresnelets for phase-shifting digital hologram compression," *IEEE Transactions on Image Processing* **15**(12), 3804–3811 (2006).

[25] A. Arrifano, M. Antonini, and M. Pereira, "Multiple description coding of digital holograms using maximum-a-posteriori," in *European Workshop on Visual Information Processing*, 232–237, (Paris, France) (2013).

[26] Y. Xing, B. Pesquet-Popescu, and F. Dufaux, "Comparative study of scalar and vector quantization on different phase-shifting digital holographic data," in *3DTV Conference*, 1–4, (Budapest, Hungary) (2014).

[27] Y. Xing, B. Pesquet-Popescu, and F. Dufaux, "Vector quantization for computer generated phase-shifting holograms," in *Asilomar Conference on Signals, Systems and Computers,* 709–713, (Pacific Grove, CA) (2013).

[28] Y. Xing, M. Kaaniche, B. Pesquet-Popescu, and F. Dufaux, "Vector lifting scheme for phase-shifting holographic data compression," *Optical Engineering, Special issue on Practical Holography: New Procedures, Materials, and Applications* **53**(11), 112312 (2014).

[29] M. Kaaniche, B. Pesquet-Popescu, and J.-C. Pesquet, "$\ell_1$ adapted non separable vector lifting schemes for stereo image coding, in *European Signal and Image Processing Conference*, 769-773, (Bucharest, Romania) (2012).

[30] 19 I. Yamaguchi, J. Kato, S. Ohta, and J. Mizuno, "Image formation in phase-shifting digital holography and applications to microscopy," *Applied Optics,* **40**(34), 6177-6186 (2001).

[31] A. Benazza-Benyahia, J.-C. Pesquet, and M. Hamdi, "Vector lifting schemes for lossless coding and progressive archival of multispectral images," *IEEE Transactions on Geoscience and Remote Sensing,* **40**(9), 2011-2024 (2002).

[32] M. Kaaniche, A. Benazza-Benyahia, B. Pesquet-Popescu, and J.-C. Pesquet, "Vector lifting schemes for stereo image coding," *IEEE Transactions on Image Processing,* **18**(11), 2463-2475 (2009).

[33] F. J. Hampson, and J.-C. Pesquet. A nonlinear subband decomposition with perfect reconstruction. In *IEEE International Conference on Acoustics, Speech and Signal Processing*, **3**, 1523–1526, (Atlanta, GA, USA) (1996).

[34] M. Kaaniche, A. Benazza-Benyahia, B. Pesquet-Popescu and J.-C. Pesquet, "Non separable lifting scheme with adaptive update step for still and stereo image coding," *Elsevier Signal Processing: Special issue on Advances in Multirate Filter Bank Structures and Multiscale Representations* **91**(12), 2767-2782 (2011).

[35] Z. Wang, A. C. Bovik, H. R. Sheikh, and E. P. Simoncelli, "Image quality assessment: From error visibility to structural similarity," *IEEE Transactions on Image Processing,* **13**(14), 600-612 (2004).

[36] G. Bjontegaard, "Calculation of average PSNR differences between RD curves," *Tech. Rep.,* ITU SG16 VCEG-M33, Austin, TX, USA (2001).

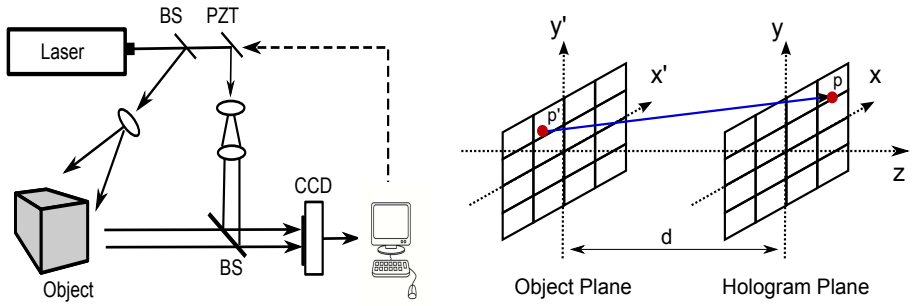


(a) (b)

Fig. 1. (a) Setup for phase-shifting digital holography: BS: beam splitters; PZT, piezoelectric transducer mirror; (b) Coordinate system of hologram recording.

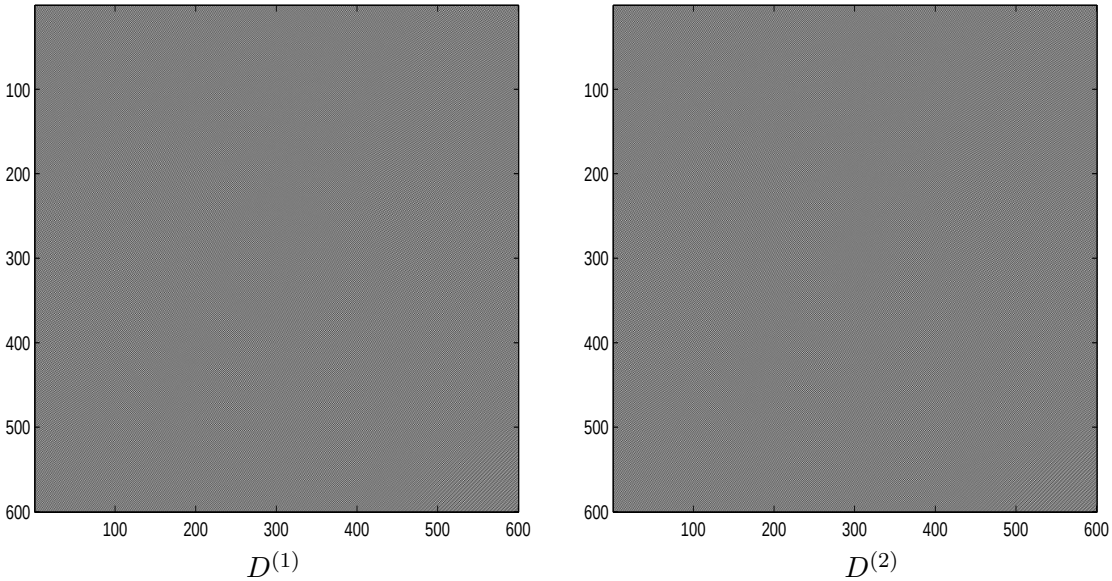


Fig. 2. Example of two difference data $D^{(1)}$ and $D^{(2)}$ for the "Bunny-1" object.

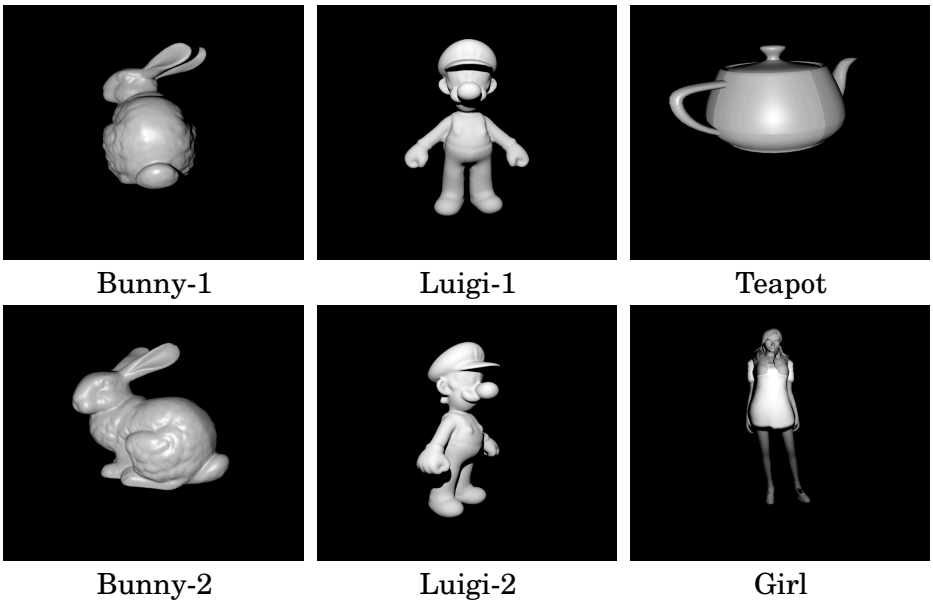


Fig. 3. Different test 3D objects

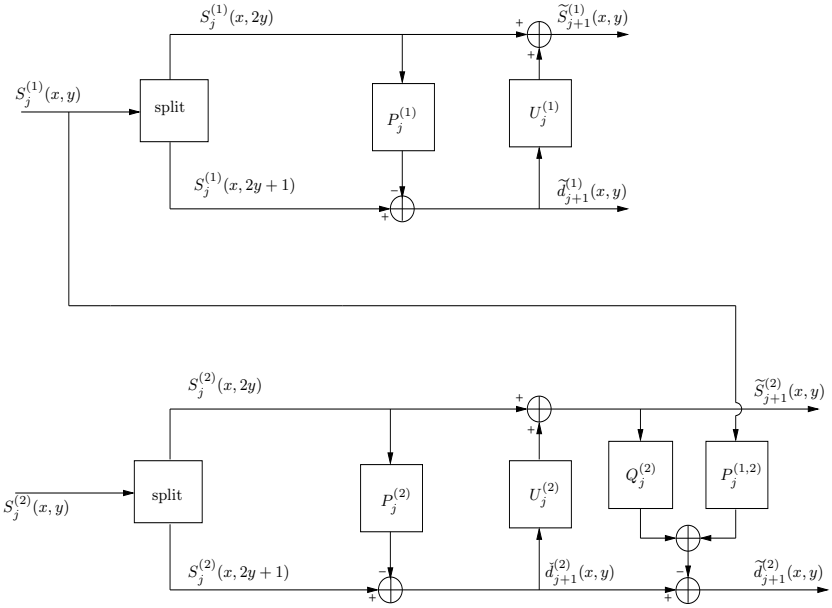


Fig. 4. Principle of the VLS decomposition.

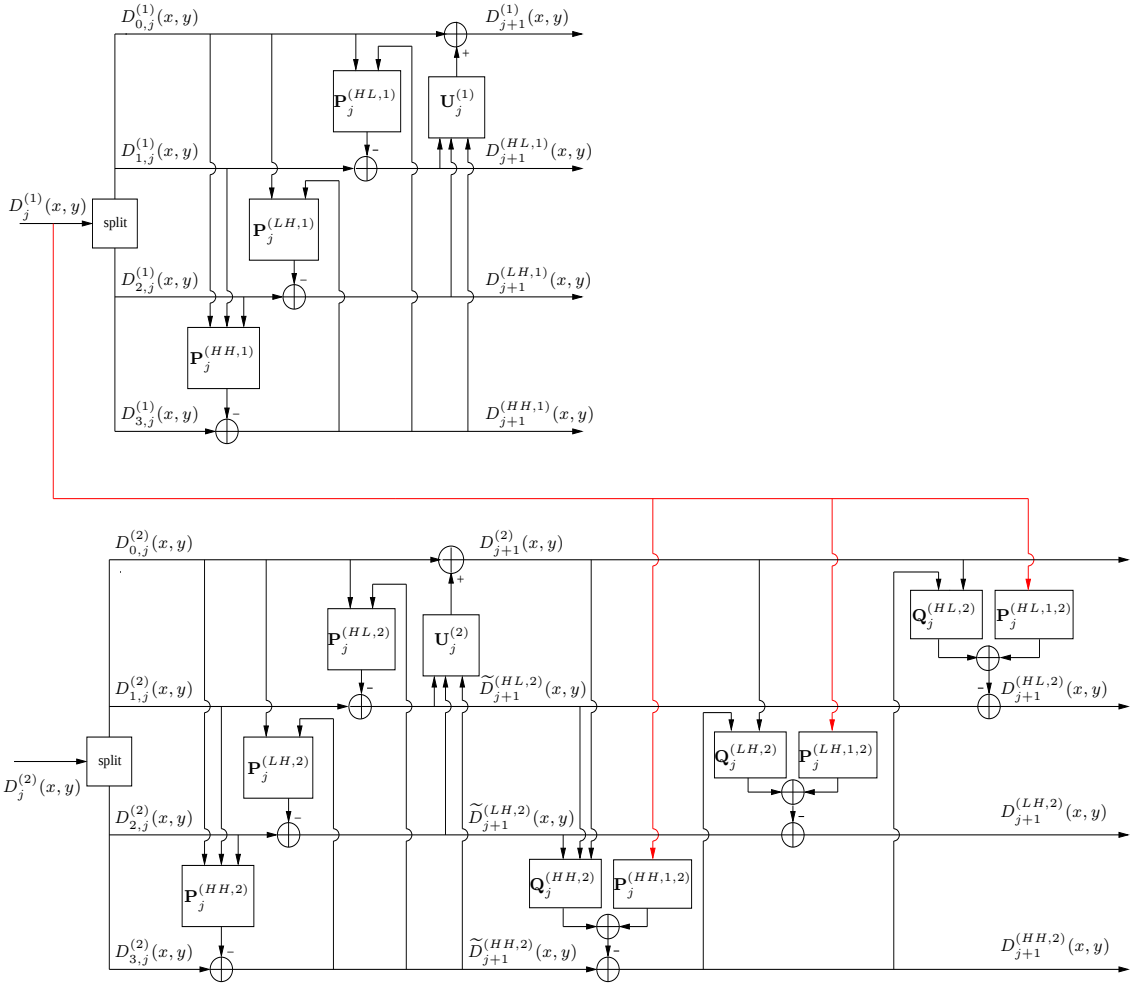


Fig. 5. Proposed NS-VLS decomposition structure.

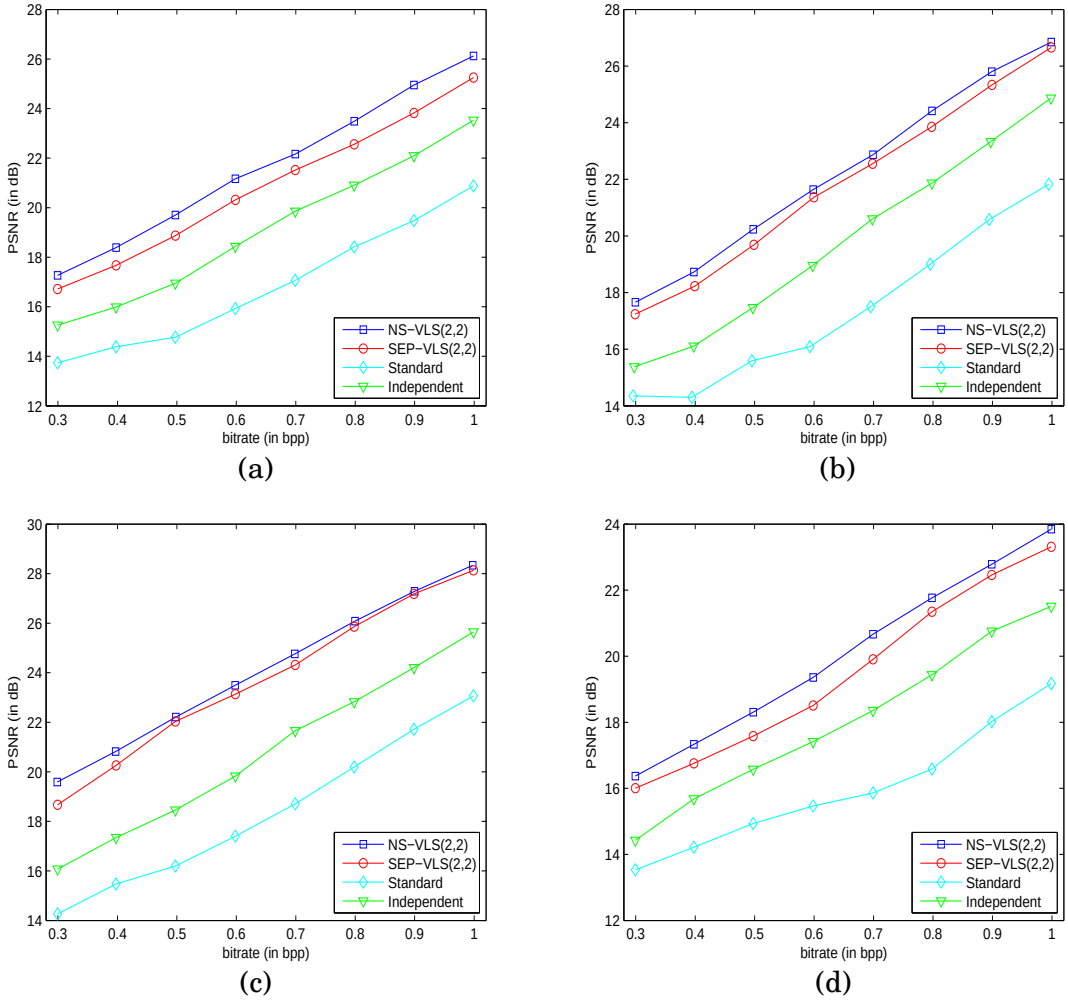


Fig. 6. Rate-distortion performance of the different hologram compression schemes for the objects: (a) “Luigi-1”, (b) “Luigi-2”, (c) “Bunny-1”, (d) “Bunny-2”.

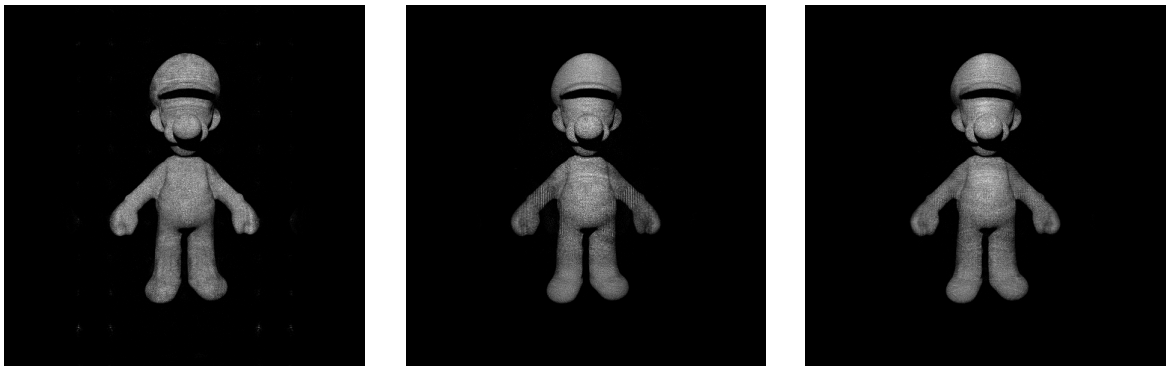

(a) PSNR=22.09 dB, SSIM=0.73 (b) PSNR=23.83 dB, SSIM=0.87 (c) PSNR=24.95 dB, SSIM=0.89

Fig. 7. Reconstructed “Luigi-1” object at 0.9 bpp using: (a) Independent, (b)SEP-VLS(2,2), (b) NS-VLS(2,2).

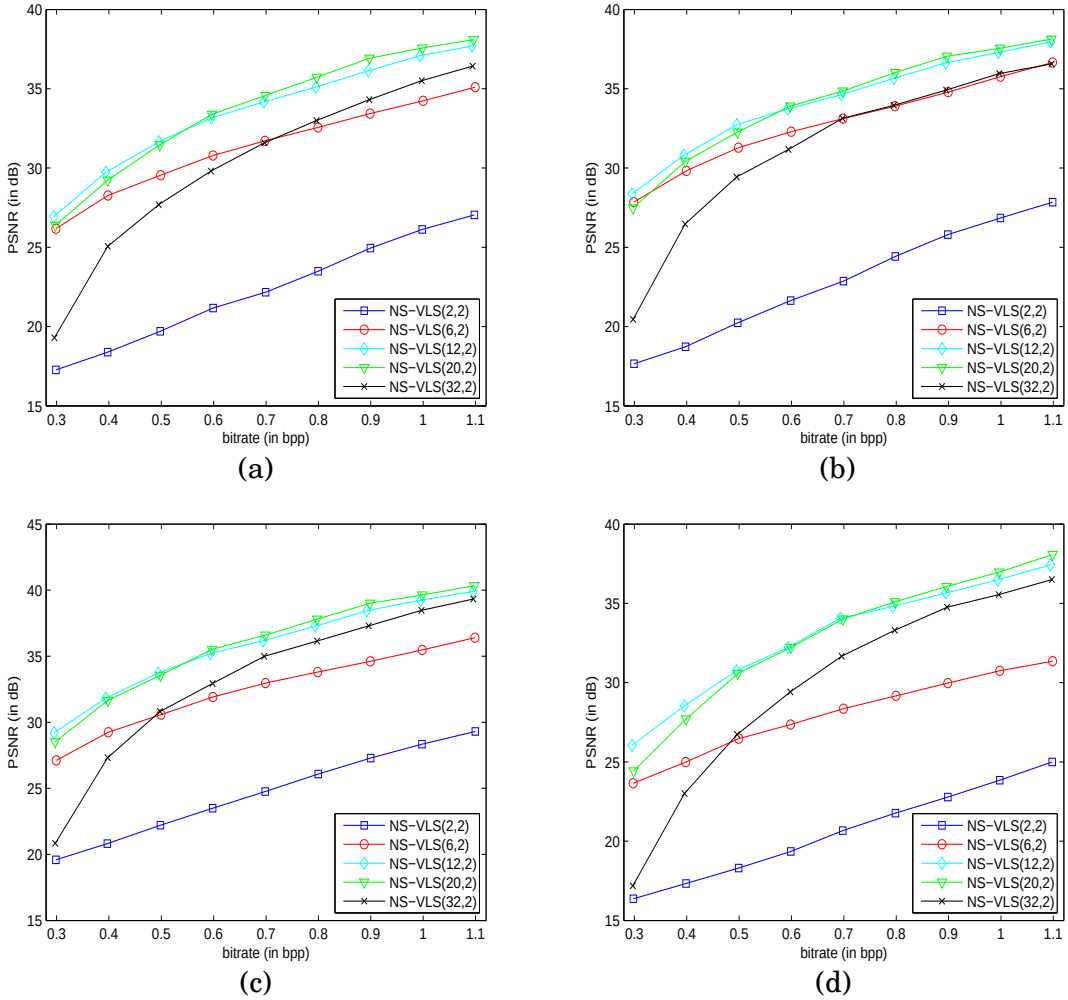


Fig. 8. Rate-distortion performance of the proposed NS-VLS with different prediction filter lengths for the objects: (a) “Luigi-1”, (b) “Luigi-2”, (c) “Bunny-1”, (d) “Bunny-2”.

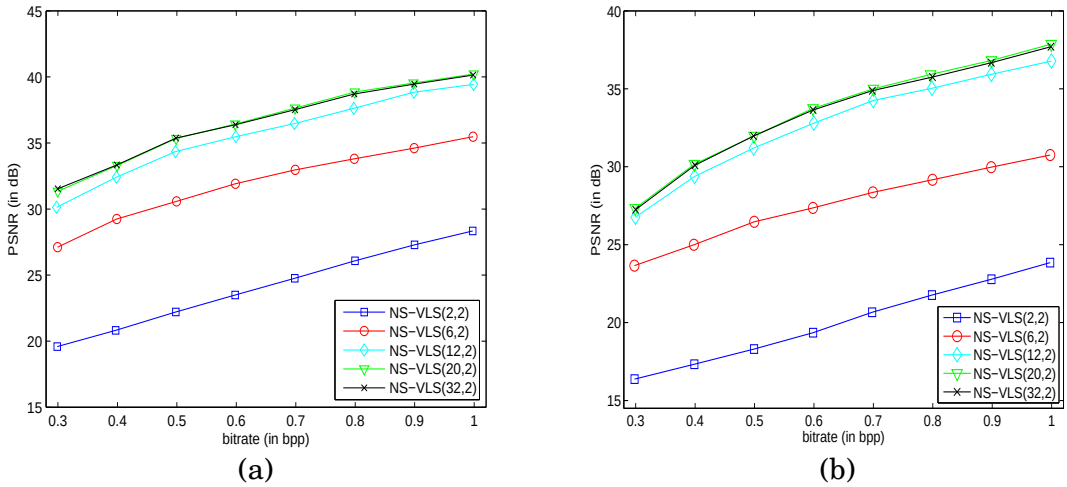


Fig. 9. Rate-distortion performance of the proposed NS-VLS with different prediction filter lengths for the objects: (a) “Bunny-1”, (b) “Bunny-2”. An example where the overhead coding cost of the filter coefficients is not taken into account.

(a)Original (b) PSNR=20.00 dB, SSIM=0.69 (c) PSNR=29.50 dB, SSIM=0.94

(d) 33.72 dB, SSIM=0.96 (e) PSNR=34.22 dB, SSIM=0.97 (f) PSNR=32.77 dB, SSIM=0.94

Fig. 10. Reconstructed “Teapot” objects at 0.8 bpp by using: (b) NS-VLS(2,2), (c) NS-VLS(6,2), (d) NS-VLS(12,2), (e) NS-VLS(20,2), (f) NS-VLS(32,2).